Journal of Physics: Condensed Matter

PAPER

Electronic structure and migration of interstitial hydrogen in the rutile phase of TiO_2

IOP Publishing Journal of Physics: Condensed Matter
J. Phys.: Condens. Matter **30** (2018) 425503 (10pp) https://doi.org/10.1088/1361-648X/aae0a2

Electronic structure and migration of interstitial hydrogen in the rutile phase of TiO_2

A G Marinopoulos, R C Vilão, H V Alberto and J M Gil

CFisUC, Department of Physics, University of Coimbra, P-3004-516 Coimbra, Portugal

E-mail: marinop@uc.pt

Received 3 July 2018, revised 8 September 2018
Accepted for publication 12 September 2018
Published 3 October 2018

Abstract

The formation and migration energies of interstitial hydrogen in rutile TiO_2 are obtained from first principles calculations. The computational approach was based on density functional theory with a semilocal generalised-gradient approximation functional, supplemented with an on-site Hubbard term to account for correlation among the Ti 3*d* electrons. Charge-transition levels are calculated and compared to previous theoretical studies. The donor character of hydrogen is examined in depth, focusing in particular on the tendency to form polaron-like configurations with the unpaired electron trapped at nearby titanium ions. Distinct minimum-energy paths of hydrogen migration and associated energy barriers were determined by the nudged elastic-band method. The present findings show clearly the strong anisotropy in the energy barriers for migration within the open *c* channels as opposed to migration crossing adjacent channels of the rutile lattice. For the rate-limiting step which leads to macroscopic diffusion along the *c* axis the corresponding rate and diffusion coefficient were also determined from transition-state theory. The results are discussed in connection to existing measurements of hydrogen diffusion and recent findings from electron paramagnetic resonance, electron–nuclear double resonance and muonium spectroscopies that probed the spatial localization of the electron spin.

Keywords: hydrogen, titanium oxide, ab initio calculations, diffusion, muon-spin rotation spectroscopy

(Some figures may appear in colour only in the online journal)

1. Introduction

The electrical activity of hydrogen in rutile TiO_2 has been the subject of debate since the 1960s where an enhancement in conductivity was reported after hydrogen was electrolytically introduced in the material [1]. There is evidence from experiments that hydrogen is a shallow donor with excitation energies of the order of a few meV [2, 3]. More recently it was reported that interstitial hydrogen in atom-hydrogenated TiO_2 introduces a shallow donor with an ionization energy of 3.9 meV [4]. Nonetheless, it was further inferred from a number of recent studies by electron paramagnetic resonance (EPR) [5], electron–nuclear double resonance (ENDOR) [5], infrared [6] and muon-spin rotation (μSR) [7, 8] spectroscopies that the neutral hydrogen atom in rutile does not possess a delocalised electron density, namely its character is not consistent with a shallow donor. Instead, it was proposed that the unpaired electron has a compact spatial distribution and is localized at a Ti site near the proton, giving rise to a Ti^{+3} defect center.

From a theory standpoint, the electrical behavior of hydrogen in the rutile phase of TiO_2 has been the subject of several first-principles studies which led to contradictory results with regard to the position of the thermodynamic charge-transition levels with respect to the conduction-band edge. Certain of these studies concluded that hydrogen is a shallow donor on account of the fact that the impurity assumes solely a positively-charged state for any Fermi-level position in the gap [9–12]. In contrast, it was reported elsewhere that

hydrogen is a deep donor with the thermodynamic $E^{\rm th}_{(0/+)}$ level positioned deep inside the band gap [13, 14]. It was further postulated that the exact amount of Hartree–Fock nonlocal exchange used in hybrid-functional approaches may be critical in driving the $E^{\rm th}_{(0/+)}$ level inside the gap [11].

The mobility and transport of hydrogen in TiO_2 is also another issue that needs a more rigorous examination from first principles. The rutile lattice presents a suitable system for generic studies of diffusion of charged ions in nonmetallic crystals owing to the existence of the *c* channels with large interstitial space which can act as easy-diffusion pathways [15]. Recent work on proton transport in rutile and its enhancement by resonant infrared light has also renewed the interest to understand better hydrogen migration mechanisms [16]. Early experimental studies [15] have reported a strong anisotropy for the activation energies of hydrogen diffusion along and perpendicular to the crystallographic *c* axis; the obtained activation energy for the latter was more than twice as large. To our knowledge no first-principles study has verified the observed anisotropy with detailed calculations of migration barriers. The most complete theoretical study of the atomistic mechanisms of hydrogen migration was performed by Bates *et al* [17] where interatomic interactions were modeled by empirical potentials. Classical barriers of migration were determined together with corrections due to zero-point motion.

The present study reports first-principles calculations of both formation and migration energies of interstitial hydrogen in rutile TiO_2. The adopted computational framework is based on density-functional theory [18, 19] in the generalized-gradient approximation (GGA) for exchange–correlation effects [20]. The on-site correlation of the Ti 3*d* electrons was also taken into account via a Hubbard-like *U*-term within a rotationally-invariant approach [21]. This GGA + *U* scheme is capable of reproducing localized polaron states in TiO_2 [11, 13, 22, 23] and represents an acceptable compromise with respect to the far more computationally expensive hybrid functionals [11, 14]. Atomistic and electronic structures of the various hydrogen configurations are resolved and compared with findings of other first-principles calculations and recent observations from EPR, ENDOR and μSR spectroscopies. The neutral charge state, in particular, is discussed in terms of the tendency of the excess electron to localize at neighboring Ti ions. Detailed migration mechanisms of hydrogen in the lattice were determined via the nudged-elastic band (NEB) method [24]. Transition-state theory [25] was further invoked to determine the jump rate and diffusion coefficient for hydrogen diffusion along the *c* axis.

2. Theoretical background and preliminaries

The calculations in the present study were based on spin-polarised density-functional theory [18, 19] and the projector augmented-wave method [26, 27], as implemented in the VASP code [28–30]. For exchange–correlation effects the GGA was assumed and the semilocal Perdew–Burke–Ernzerhof functional was employed [20]. A Hubbard-type on-site term *U* was also added according to the rotationally-invariant scheme by Dudarev *et al* [21] in order to account for the correlation between the Ti 3*d* electrons. A magnitude of 4.2 eV was chosen for *U*, matching corresponding *U* values from earlier studies [11, 22, 31]; this specific choice led to better agreement with experimental spectroscopies regarding the defect states of oxygen vacancies at TiO_2 surfaces. The crystalline wavefunctions for the valence electrons were expanded in a plane-wave basis up to a kinetic-energy cutoff of 470 eV. For titanium the 3*p*, 4*s* and 3*d* states were treated as valence states, leaving [Ne] and 3*s* in the core. For oxygen the 2*s* and 2*p* were treated as valence states.

For the bulk primitive cell of TiO_2 the optimization was carried out using a Γ-centered $7 \times 7 \times 7$ **k**-point mesh. The energy minimization led to lattice parameters *a* and *c* equal to 4.67 Å and 3.03 Å, respectively. A magnitude of 2.25 eV for the band gap was also obtained. This underestimates the experimental gap of 3.037 eV [32] but is consistent with results of previous GGA + *U* calculations [11, 31].

The defect calculations were performed using a 96-atom supercell that was constructed from a $2 \times 2 \times 4$ repetition of the primitive tetragonal unit cell of rutile along the lattice vectors. 4 **k** points were used for the Brillouin zone integrations. Additional calculations using a larger $3 \times 3 \times 4$ supercell (of 216 atoms) were also performed for calculating the formation energies of hydrogen. A broader mesh was used in this case with 2 **k** points in the Brillouin zone: (0,0,0) and (1/2,1/2,1/2). The calculations of the electronic density of states (DOS) were performed for the 96-atom supercells using a finer, $5 \times 5 \times 5$, **k**-point mesh.

The formation energies $E_{\rm form}(H^q)$ of the three different charge states *q* of hydrogen ($q = -1, 0$ and $+1$) were determined as a function of the electron chemical potential (Fermi level $E_{\rm F}$) in the gap:

$$E_{\rm form}(H^q) = E_{\rm tot}(H^q) - E_{\rm tot}({\rm bulk}) - \mu_{\rm H} + q(E_{\rm F} + E_{\rm V}) \quad (1)$$

where $E_{\rm tot}(H^q)$ is the total supercell energy with a single hydrogen present in the charge state *q*, and $E_{\rm tot}({\rm bulk})$ the total energy of the bulk-crystalline supercell. $\mu_{\rm H}$ is the chemical potential of hydrogen and was taken as half the total energy of an isolated hydrogen molecule at $T = 0$ K. This choice corresponds to hydrogen-rich conditions. $E_{\rm V}$ is the energy of the valence band top of the bulk supercell and defines the reference energy for the Fermi-level positions in the gap. Owing to the very large magnitude of the ionic part of the dielectric constant [33] no electrostatic corrections were applied to the calculated formation energies.

The migration paths for hydrogen and corresponding energy profiles were determined from the NEB method [24]. From the NEB results both the classical migration barriers and saddle points (transition states) along the paths were deduced. In all NEB calculations hydrogen was assumed to be in its positively-charged state, H^+. This assumption is consistent with the fact that the emphasis in the present study has been to compare with earlier high-temperature diffusion data where hydrogen was ionized, namely existed as a proton defect (H^+ charge state) [15]. Tests for the migration barriers of H^0 in

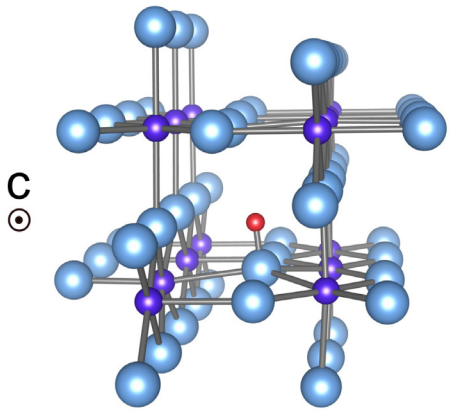

Figure 1. Atomistic structure of the positively-charged hydrogen configuration, H^+. This is a basal-plane view along the channel (parallel to the *c* axis). The chemical elements in this figure (and the figures to follow) are represented as: H (very small red sphere), Ti (small dark-magenta spheres) and O (large blue spheres).

the in-channel paths led to barriers close to the those of H^+ to within 0.02 eV.

The calculations of the vibrational frequencies were performed within the harmonic approximation for lattice vibrations. The Hessian force–constant matrix was initially constructed by finite differences of the forces allowing for small displacements of all atoms within a radius of 3.5 Å around the hydrogen site. From the diagonalization of the Hessian matrix the normal-mode frequencies were obtained for the ground-state and transition-state configurations.

3. Results

3.1. Defect levels and electron trapping

Similarly to existing first-principles calculations hydrogen in its positively-charged state, H^+, was observed to bind to oxygen ions in hydroxide-ion configurations: it forms short dative-type O–H bonds, with a O–H bondlength equal to 0.99 Å, oriented perpendicular to the *c* axis (see figure 1). This is consistent with previous experiments of polarized infrared (IR) spectroscopy which showed that the electric dipole axis (defined by the bond direction) lies on the basal *ab* plane of the rutile lattice [34]. As was already recognized previously [9, 35] the incorporation of hydrogen in the lattice does not lead to breaking of any metal–oxygen bonds of the host; the oxygen ions retain their three-fold cation coordination. In figure 1 it can be seen that the oxygen ion participating to the O–H bond (to be referred as O_{nn}) forms also bonds with three Ti ions. The Ti neighbor on its left belongs to the same basal plane with this oxygen (in-plane Ti_{in}), whereas the two Ti neighbors on the right do not (out-of-plane Ti_{out}'s). Nonetheless, the formation of the O–H bond causes local displacements of the oxygen ion O_{nn} and of its three nearest Ti neighbors. As a result the three Ti–O_{nn} bonds become elongated (with a length equal to 2.14 Å) compared to the bulk crystal where the Ti_{in}–O distance is equal to 1.99 Å and the distance Ti_{out}–O to the two out-of-plane Ti neighbors is 2.015 Å.

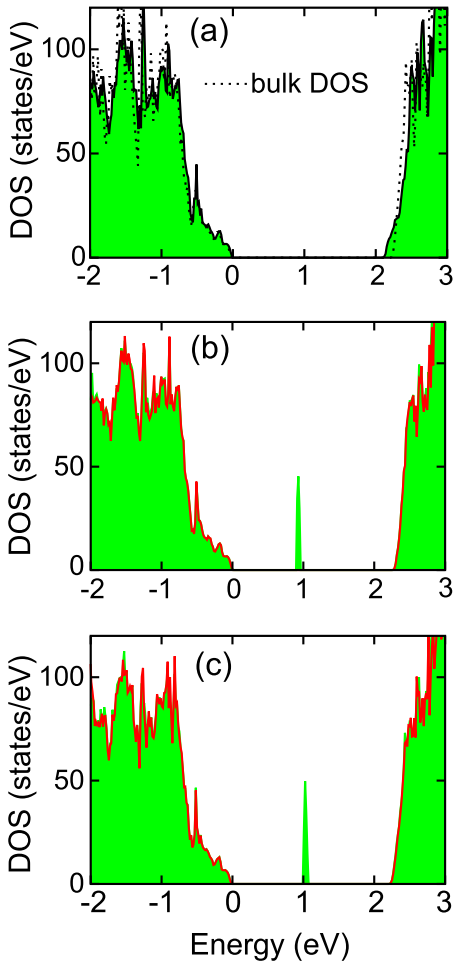

Figure 2. Total electronic DOS for the minimum-energy neutral hydrogen configurations. (a) Delocalized configuration. The dashed line denotes the DOS for the bulk supercell. (b) Ground-state localized configuration with the electron at the out-of-plane Ti ion. (c) Localized configuration with the electron at the in-plane Ti ion. The results shown in (b) and (c) are spin-polarized calculations with the spin-up component denoted with the filled green color (no line) and the spin-down component with the red line. The zero-energy reference is the valence-band top. The DOS plots are presented with an energy smearing value of 0.1 eV.

Furthermore, some of the distances between these Ti ions with the other five oxygen ions in the TiO_6 octahedra are shortened and become as low as 1.90 Å. Overall, these displacements appear to be driven by the need to minimize the strong repulsion of H^+ with the closest positively-charged Ti ions. Adding a single electron to this configuration creates a stable H^0 state inducing virtually no structural relaxation. Examination of the partial electron density for hydrogen showed that the density is delocalized in the whole supercell. The DOS plot for this configuration does not reveal any defect deep levels inside the gap (see figure 2(a)). Instead, hydrogen induces a resonance in the bottom of the conduction band (CB) which protrudes below the bulk-crystalline CB edge. The calculated Fermi level lies inside this resonance, thus suggesting a very small excitation energy for the creation of H^+ and the release of the electron to the CB.

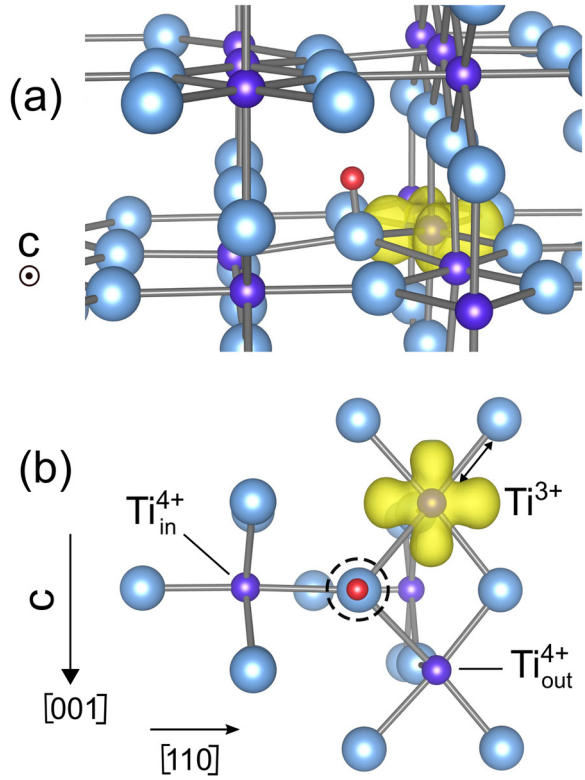

Figure 3. Atomistic structure of the neutral hydrogen configuration with the excess electron localized at the out-of-plane Ti ion. The spin-density isosurface is shown in yellow with a corresponding isovalue equal to 0.009 e $Å^{-3}$. (a) Basal-plane view along the channel (parallel to the *c* axis; [0 0 1] projection). (b) View perpendicular to the *c* axis. The dashed circle denotes the O–H bond. The double-sided arrow line shown alongside the Ti–O bond indicates an elongation of the respective bondlength compared to the H^+ state, where it was equal to 1.90 Å. Subscripts in and out denote in-plane and out-of-plane Ti ions.

Nonetheless, this delocalized H^0 state is not the thermodynamically lowest-energy state of neutral hydrogen. Subsequent optimization showed that lower-energy solutions exist with the excess electron localized on individual Ti ions near the O–H bond. These H^0 configurations are polaron-like: local lattice distortions near the Ti sites are necessary to localize the electron at these sites rendering the initial Ti^{+4} ion to a Ti^{+3} defect center. Similarly, previous calculations by both GGA + *U* and hybrid-functional approaches [11, 13, 14, 23] showed that such localized solutions exist with the excess electron trapped at different Ti sites. In agreement with one of these earlier works which presented a systematic listing of possible localized solutions of hydrogen states [23] the present study concludes that the lowest-energy H^0 configuration is the one with the electron localized on the out-of-plane Ti ion nearest to the O–H bond (see figure 3). It can be seen from the plotted spin density and population analysis that the excess electron is of *d* character. The charge distribution has a planar four-lobe shape with the plane defined by the four nearest O neighbors. The lobe axes point along the [0 0 1] and [1 1 0] directions and cut midway the O–Ti–O angles. The corresponding defect state appears as a deep level in the mid-gap region, at approximately 1.3 eV below the CB (see figure 2(b)). In the previous GGA + *U* studies the hydrogen-induced states were also in the mid-gap region, although the specific position depended on the chosen *U* value [11, 23]. For $U = 2.5$ eV the defect states were found to lie within a range of 0.8–1.0 eV below the CB [23], whereas for $U = 4.2$ eV the corresponding range was at 1.1–1.3 eV below the CB [11]. The hydrogen-induced defect state predicted by the hybrid HSE06 functional was found closer to the CB, at approximately 0.8 eV below the CB [11].

The distances of the Ti^{+3} ion to its closest O neighbors range from 2.03 Å to 2.08 Å, whereas the distance of Ti^{+3} to the O_{nn} ion which forms the O–H bond equals 2.17 Å (see figure 3). The Ti–O bond which was compressed in the H^+ configuration (of length equal to 1.90 Å) is explicitly shown by the double-sided arrow line in figure 3. Therefore, the longer Ti–O separations appear to be necessary in order to trap the electron at the specific Ti site. It is noteworthy to mention that in the previous studies with GGA+*U* and hybrid-functional approaches in TiO_2 the excess electron in the polaron-like ground states was either bound at more distant Ti ions from the O–H bond [11, 13] or even shared among two different Ti ions nearby [14].

A recent experimental study [5] reporting measurements in rutile TiO_2 using EPR and ENDOR techniques proposed that the unpaired electron of the neutral hydrogen donor is localized on an adjacent in-plane Ti ion on the same basal *ab* plane as the O–H bond, and along the [1 1 0] direction. It was argued that such a geometry can explain the small measured hyperfine interaction with the hydrogen nucleus, in particular the vanishingly small Fermi-contact term and the predominance of the dipolar components in the hyperfine matrix [5]. Spectroscopic μSR measurements using muons also confirmed this proposal by studying the formation of muonium (a light pseudoisotope of hydrogen) in rutile TiO_2 [7, 8]. The present calculations indeed determined such a H^0 configuration which was found to be a local energy minimum (see figure 4), but with an energy higher to the one of the ground-state H^0 configuration depicted in figure 3 by 0.11 eV. The fact that the spin density is not centered on the hydrogen nucleus is consistent with the small Fermi-contact term, as observed experimentally [5, 8].

The fact that this high-energy configuration matches the experimental observations is not straightforward to reconcile. Although μSR spectroscopy is known to probe higher-energy muonium states as well, EPR should very likely identify the true ground state at thermodynamic conditions. Possible explanations can be the presence of other defects (oxygen vacancies) which may associate with hydrogen or the rather high hydrogen concentration in the EPR measurements. This may have given rise to non negligible hydrogen–hydrogen interaction which could stabilize the electron at the in-plane Ti site. Furthermore, it is possible that more complicated displacement patterns around the impurity may be necessary to stabilize by means of DFT calculations a lower-energy polaron-like configuration with the electron localized at the in-plane Ti ion. This, however, has not been possible in the present study. It is also relevant to note that previous GGA+*U*

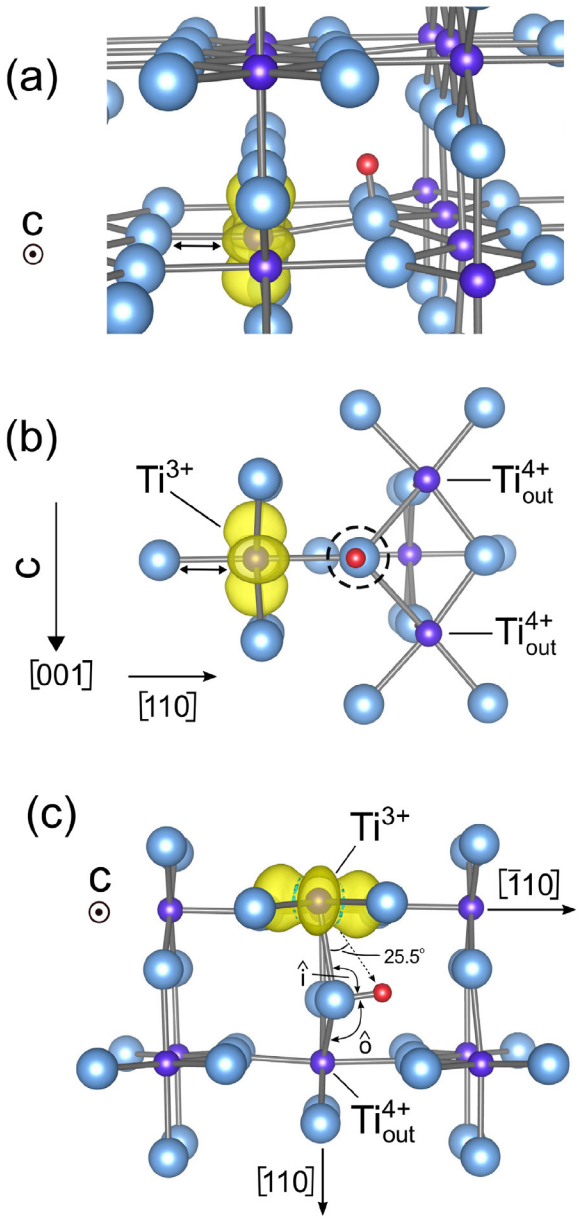

Figure 4. Atomistic structure of the neutral hydrogen configuration with the excess electron localized at the in-plane Ti ion. The spin-density isosurface is shown in yellow with a corresponding isovalue equal to 0.009 e Å^{-3}. (a) Basal-plane view along the channel (parallel to the *c* axis; [0 0 1] projection). (b) View perpendicular to the *c* axis. The dashed circle denotes the position of the O–H bond. (c) Basal-plane view along the channel with the structure relaxed by taking the experimental lattice parameters. The double-sided arrow line shown alongside the Ti–O bond indicates an elongation of the respective bondlength compared to the H^+ state, where it was equal to 1.90 Å. Subscript out denotes the out-of-plane Ti ions.

calculations [23] also identified the configuration with the electron localized at the in-plane Ti ion as being of higher energy; no explicit information on the local structure or on the spin-density distribution was presented though.

As it can be seen in figure 4 from the spin-density isosurface it can be inferred that the unpaired electron possesses a *d*-type character with a planar four-lobe structure. The defect-induced state also appears as a deep level inside the gap (see figure 2(c)). Figure 4(c) presents another detailed view of this configuration showing the planar spin distribution on the plane defined by the [1 1 0] and [$\bar{1}$ 1 0] directions. This basal-plane view allows a better comparison with the structure proposed previously on the basis of EPR and μSR spectroscopies [5, 8]. In order to compare with experiment the structural optimization was repeated using the experimental lattice parameters for rutile TiO_2. The lobe axes point along the [0 0 1] and [$\bar{1}$ 1 0] directions, in perfect agreement with the ENDOR analysis which also concluded that the unpaired electron occupies a *d*-type $|\, x^2—y^2 >$ orbital with the *x* and *y* axes defined by the [$\bar{1}$ 1 0] and [0 0 1] directions, respectively [5].

The three Ti–O_{nn} distances are equal to 2.14 Å as in the H^+ state. The distances of the Ti^{+3} ion to its six nearest O neighbors in this configuration are in the 1.96–2.14 Å range. The Ti–O bond which was compressed in the H^+ configuration (of length equal to 1.90 Å) is explicitly shown by the double-sided arrow line in figure 4. It can be seen in figure 4(c) that the oxygen ion O_{nn} which bonds with hydrogen is equidistant to the two nearest Ti ions, the in-plane Ti^{+3} and the out-of-plane Ti^{+4}, with the respective distance equal to 2.08 Å. The Ti^{+3}–H distance is slightly longer (2.32 Å). The angles $\hat{\imath}$ and $\hat{o}$ are equal to 90.7° and 102.5°, revealing an asymmetry in the orientation of the O–H bond with respect to the Ti^{+3} and Ti^{+4} nearest neighbors. Namely, the O–H bond is skewed towards the Ti^{+3} ion, very likely due to the smaller positive charge with respect to Ti^{+4}. The arrowed line in figure 4(c) which starts from Ti^{+3} and points to H forms a 25.5° angle with the Ti^{+3}–O_{nn} bond direction. The corresponding angle is bigger (34.8°) if measured with respect to the [1 1 0] axis owing to a small tilt of the Ti^{+3}–O_{nn} bond with respect to [1 1 0]. In the interpretation of Brant *et al* [5] this line points closely to the direction of the principal axis of the hyperfine interaction that lies on the basal plane. Their analysis of the ENDOR spectra led to a value of 22.9° for the angle between the principal axis and the [1 1 0] direction.

Subsequent calculations varying the magnitude of *U* showed that the energy difference between the two polaron-like configurations does not change and the configuration depicted in figure 3 remains the ground state of H^0 even down to a value of *U* equal to 2 eV. Below this value both localized H^0 configurations transform into the delocalized H^0 state, with the excess electron occupying the bottom of the CB and spatially delocalized in the whole supercell. This shows that a minimum finite value of on-site correlation *U* is needed to stabilize the localized solutions in favor of the delocalized one.

Finally, in the H^- state hydrogen also binds to the oxygen ions adopting a geometry nearly identical to the one of the H^+ state.

Taking the lowest-energy configuration for each charge state of hydrogen the defect formation energies can be subsequently obtained with respect to the Fermi-level position in the band gap. The resulting plot is displayed in figure 5. The negatively-charged H^- state is not thermodynamically stable for any value of the Fermi level and the acceptor level, $E^{\rm th}_{(0/-)}$, is found inside the CB. Instead, the thermodynamic donor level, $E^{\rm th}_{(+/0)}$, lies well within the gap: $E^{\rm th}_{(+/0)} = E_{\rm C} - 0.43$ eV, where $E_{\rm C}$ is the CB edge. This result shows that hydrogen is

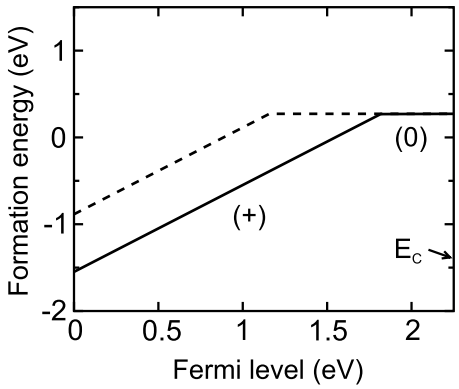

Figure 5. Formation energy of interstitial hydrogen in TiO_2 as a function of the Fermi-level position in the gap, for hydrogen-rich conditions. The reference for the Fermi level is the valence-band top, E_V. E_C denotes the calculated conduction-band edge. The dashed lines refer to the charge states involved in the optical (vertical) excitation process (see text).

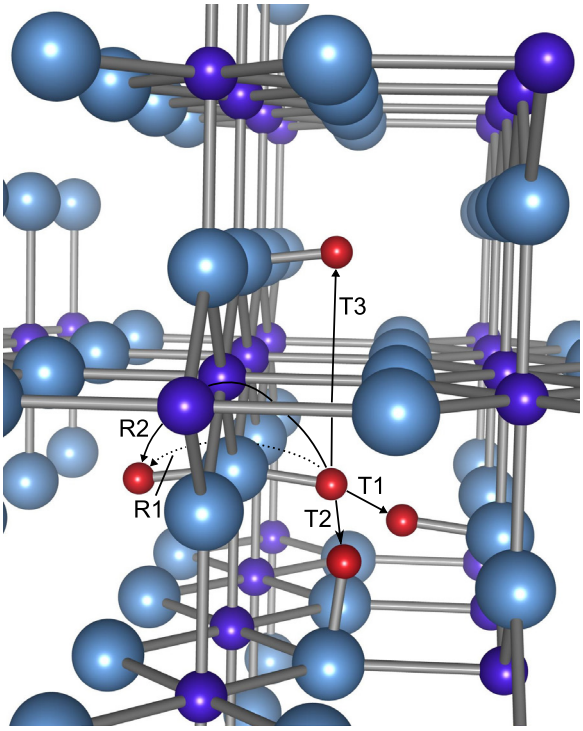

Figure 6. Hydrogen migration paths in the rutile lattice. The paths are denoted by the arrows and connect initial and final (after migration) positions of the hydrogen. Initial and final hydrogen sites are isoenergetic. T1, T2 and T3 are transfer-type modes, whereas R1 and R2 are bond-reorientation modes. The view is along the *c* channels, parallel to the crystallographic *c* axis.

a deep donor in rutile and agrees with earlier first-principles studies that also place this level inside the gap [13, 14]. In particular, the hybrid HSE06 calculations by Deák *et al* [14] place this level at 0.5 eV below the CB, whereas the GGA+U calculations by Filippone *et al* [13] even deeper inside the gap.

The optical charge-transition level, $E^{\rm opt}_{(+/0)}$, can also be obtained by assuming a vertical excitation process; namely, that ionization towards the positively-charged state happens so fast that H^+ still adopts the equilibrium geometry of H^0.

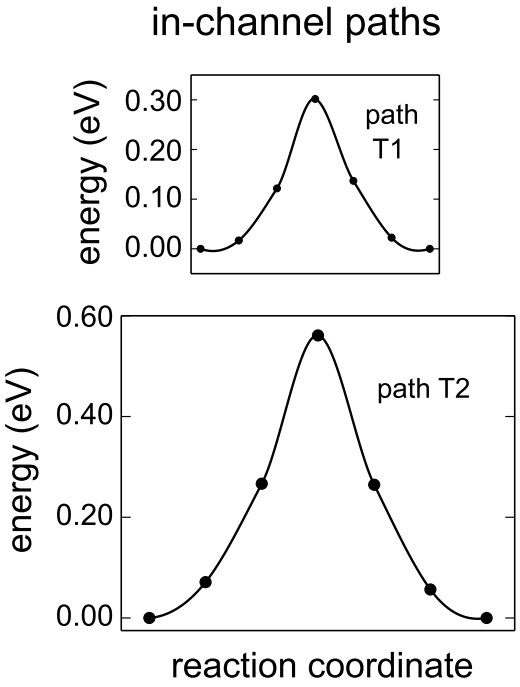

Figure 7. Energy profiles for proton migration along the in-channel paths in the TiO_2 lattice. The curves were generated from interpolation of the exact results (filled circles) obtained from the NEB calculations. The abscissa magnitudes in the graphs are proportional to the total hydrogen displacements.

The optical level, as expected, is even deeper compared to the thermodynamic level: $E^{\rm opt}_{(+/0)} = E_C - 1.09$ eV (see figure 5). This result is in good agreement with two hybrid-functional calculations [11, 14] which predict a position for the optical donor level in rutile at: $E^{\rm opt}_{(+/0)} = E_C - 0.82$ eV.

In contrast to the present results, existing GGA + U calculations have predicted an acceptor level, $E^{\rm th}_{(0/-)}$, deep inside the gap [13]. This discrepancy may originate from the fact that these authors used the experimental band gap as the range of Fermi levels without correcting the charge-dependent formation energies [13]. It is relevant to note, furthermore, that experimentally there is no evidence for the formation of negatively charged H^- (or Mu^-) in previous measurements done in *n*-type rutile samples either hydrogenated or implanted with muons [7, 8].

3.2. Atomistic mechanisms of hydrogen migration

The NEB calculations identified a number of distinct migration paths for hydrogen which can be grouped in two categories: in-channel paths whereby hydrogen displacements are confined inside the *c* channels, and cross-channel paths where hydrogen crosses between adjacent channels, thus achieving a long-range motion on the basal *ab* planes, perpendicular to the crystallographic *c* axis. All migration paths are depicted schematically in figure 6 as arrows connecting initial and final hydrogen positions before and after migration, respectively. The initial and final hydrogen sites in these paths are isoenergetic. The calculated energy profiles along the paths are

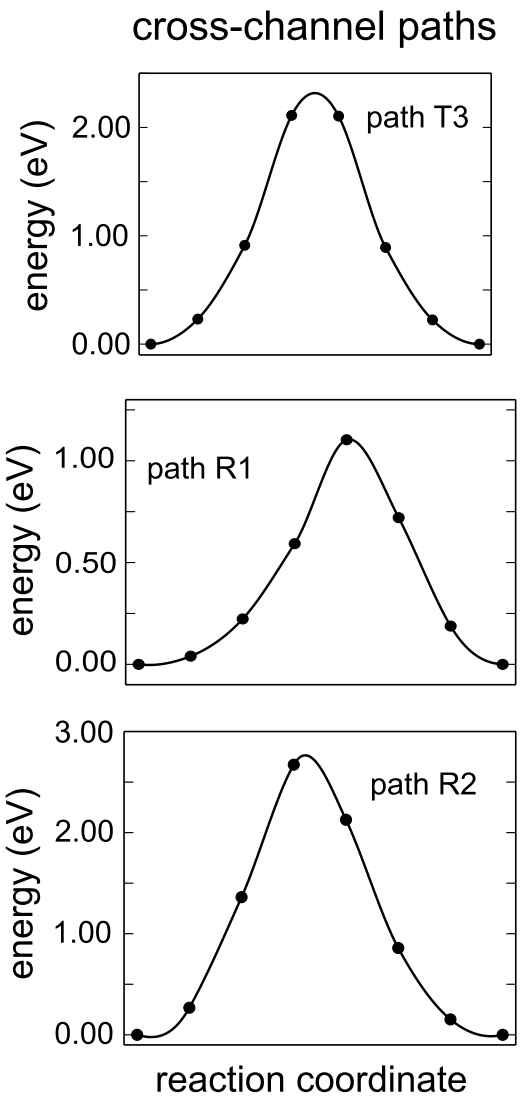

Figure 8. Energy profiles for proton migration along the cross-channel paths in the TiO_2 lattice. The curves were generated from interpolation of the exact results (filled circles) obtained from the NEB calculations.

Table 1. Migration barriers, $E_{\rm barr}$, of hydrogen in rutile. Results in parentheses denote the barriers with the zero-point energy correction (values in eV).

In-channel paths	
T1	0.30 (0.17)
T2	0.56 (0.44)
Cross-channel paths	
T3	2.30
R1	1.10 (1.06)
R2	2.75

displayed in figures 7 (in-channel paths) and 8 (cross-channel paths). The obtained migration barriers, $E_{\rm barr}$, for all paths are listed in table 1. These barriers are calculated as the difference of total DFT energies between the transition-state (TS) and the initial (before the jump) ground-state (GS) configurations. Namely:

$$E_{\rm barr} = E_{\rm tot}^{\rm TS} - E_{\rm tot}^{\rm GS}. \quad (2)$$

The paths for hydrogen motion within the channels are denoted as T1 and T2 (see figure 6). Both of them are proton-transfer type paths with hydrogen hopping between neighboring oxygen ions. In the first path (T1) hydrogen hops perpendicular to the c axis and does not change its c-axis coordinate after the completion of the jump. Thererefore, it cannot contribute to long-range diffusion along the channels. This path is the shortest among all paths encountered in the present study with a total hydrogen displacement of 0.92 Å. The associated energy profile is nearly symmetric and the energy barrier $E_{\rm barr}$ is very low (equal to 0.30 eV) (see figure 7). Since the activation energy, $E_{\rm a}$, for hydrogen migration can be represented to a first approximation by the classical barrier $E_{\rm barr}$, such a small value clearly suggests that the barrier along T1 can be easily overcome by hydrogen even at low temperatures. A correction, $\delta E_{\rm ZPE}$, due to the zero-point motion of hydrogen can even lower more $E_{\rm a}$ ($\delta E_{\rm ZPE}$ is negative), according to: $E_{\rm a} = E_{\rm barr} + \delta E_{\rm ZPE}$. The zero-point energy (ZPE) correction is obtained as follows [36]:

$$\delta E_{\rm ZPE} = \sum_i \frac{h\nu_i^{\rm TS}}{2} - \sum_i \frac{h\nu_i^{\rm GS}}{2}. \quad (3)$$

The vibrational frequencies $\nu_i^{\rm GS}$ and $\nu_i^{\rm TS}$, in equation (3) correspond to normal modes of vibration i and were determined from the diagonalization of the dynamical matrices of the system with hydrogen occupying the initial (GS) and saddle-point (TS) positions, respectively. The size of these matrices, $3N \times 3N$, was defined by assigning a radius of 3.5 Å around hydrogen and allowing only the N atoms within this sphere to be displaced. The total number of atoms, N, included in the present case was equal to 20.

The calculated ZPE correction for the T1 path was found equal to −0.13 eV, thus lowering the activation energy for hydrogen migration to 0.17 eV. Owing to the short-range character and the low $E_{\rm a}$ of T1, hydrogen can be thought to hop easily back and forth between the two energy minima which are the end points of this path. This motion effectively resembles a confined vibration within a symmetric double-well potential. It was argued in the past that hydrogen in rutile TiO_2 may be assumed to occupy a modified channel-centered (MCC) site [37] which is in fact the saddle point of the T1 path (namely the middle of the path). In this case the MCC site should be viewed as the time-average site of hydrogen while it performs the jumps along the T1 path.

The second in-channel path (denoted T2) is also a transfer-type path, but now the hydrogen jump length is longer (equal to 1.51 Å) and the corresponding displacement has a predominant component along the c axis; thus, T2 will contribute to macroscopic diffusion along the channels. The corresponding energy barrier is equal to 0.56 eV, a value close to previous results based on plain DFT (GGA without U correction) and GGA+U approaches [13, 38]. The ZPE correction for the T2 path is −0.12 eV and lowers the activation energy for migration to 0.44 eV.

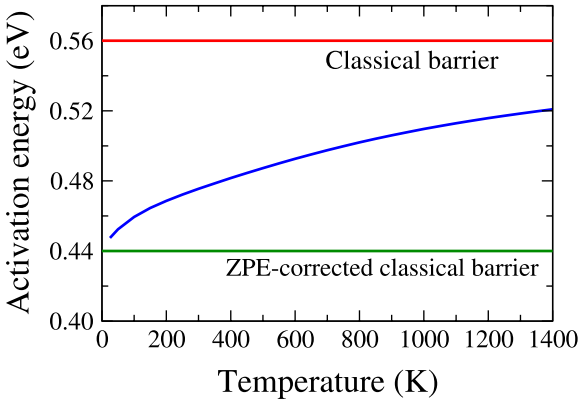

Figure 9. Calculated activation energy E_a for hydrogen diffusion along the c axis. Horizontal lines denote the classical migration barrier E_{barr} (as obtained from the NEB calculations) and the same barrier corrected with the ZPE. The temperature-dependent curve represents the sum of E_{barr} and the quantum-mechanical Wigner correction δE_{Wigner}.

For cross-channel motion three distinct hydrogen paths were identified. Two of them are bond re-orientation modes (R1 and R2) and the third one (T3) is a proton-transfer type (see figure 6). The energy barriers for these paths are consistently larger to those of the in-channel paths (see figure 8 and table 1). Even accounting for ZPE correction for the R1 mode (which has the smallest E_{barr} among the three cross-channel modes) cannot make the respective activation energies comparable to the ones of the in-channel paths (see table 1).

This finding demonstrates the strong anisotropy in the migration of hydrogen and agrees with the existing experimental diffusion data [15, 38]. More specifically, the energy barrier E_{barr} for the proton-transfer T3 path is extremely high (2.30 eV), very likely owing to the rather large hopping length for hydrogen (equal to 2.89 Å). This shows that in-plane diffusion of hydrogen across the channels (perpendicular to the c axis) cannot be accomplished through proton transfer; instead, rotational-type motion with reorientation of the O–H bonds needs to be invoked (see figure 6). In the first rotational mode (denoted R1) the angle between the O–H bond and the c axis varies between $-90°$ to $90°$. The proton needs to pass through oxygen ions to complete the full rotation covering a total displacement of 2.45 Å, measuring the distance between its initial and final sites. Such a rotation is not so penalizing energetically, and the corresponding energy barrier is equal to 1.10 eV, considerably smaller to the one of the proton-transfer T3 path.

In the second rotational mode (R2) the O–H bond remains always perpendicular to the c axis during the rotation process, namely the proton motion is confined to the basal ab plane (see figure 6). This mode possesses an extremely high energy barrier (equal to 2.75 eV) probably related to the fact that the proton has to pass between two Ti^{+4} ions to complete the path. The corresponding Ti–H^+ distances at the saddle point are 1.80 Å, thus increasing the mutual repulsion and the total energy.

The present results also lend support to a recent analysis of muonium motion in rutile TiO_2 [8]. In that study muon-spin-rotation spectroscopy was performed and the formation of muonium (a light isotope of hydrogen) and subsequent dynamics were monitored. It was argued that the disappearance of the hyperfine interaction at low temperatures was due to muon hopping along the c channels. This interpretation is justified from the present results. Within a harmonic approximation for zero-point motion [39] the ZPE correction for muonium can be obtained by scaling the respective correction for hydrogen by the factor $\sqrt{m_p/m_\mu}$. Since: $m_\mu = 0.113 m_p$ this factor equals 2.98. Therefore the ZPE correction for muonium amounts to 0.40 eV and 0.36 eV for the T1 and T2 paths, respectively. This means that the T1 path is virtually invisible to the muon while the activation energy for muon migration along the T2 path (namely along the c channels) reduces to 0.20 eV. This reduction will aid muon motion along the c channels. In contrast, the very high energy barriers of the cross-channel paths will remain insurmountable for the muon even after taking into consideration any ZPE corrections.

3.3. Diffusion rate and coefficient along the c axis

Absolute rate theory, also known as transition-state theory (TST) describes the thermally-activated movement of defects in solids within classical statistical mechanics [25]. Accordingly, the hopping rate, Γ, for an interstitial impurity diffusing in a lattice can be expressed within TST as a product of an effective frequency ν_* and an activation exponential. It was shown that for small vibrations and within the harmonic approximation ν_* can be written as the ratio of products of the real frequencies of the system when hydrogen occupies corresponding sites at the GS and TS configurations [25]. Accordingly the rate Γ can be expressed as:

$$\Gamma = \left(\frac{\prod_i^{3N} \nu_i^{GS}}{\prod_i^{3N-1} \nu_i^{TS}} \right) \times e^{-E_a/k_B T} \qquad (4)$$

where it should be stressed that the GS configuration possesses $3N$ real frequencies ν_i^{GS}. The TS configuration instead has $3N-1$ ones (denoted by ν_i^{TS}), since the frequency along the direction of the path is imaginary.

For hydrogen migration along the c axis it is the path T2 which gives rise to long-range macroscopic diffusion (see figure 6). The corresponding migration barrier for this path equals 0.56 eV (see table 1). This value is slightly higher to the result (equal to 0.52 eV) obtained by plain DFT (conventional GGA functional without U-correlation correction) [38]. On the other hand it agrees better with findings of another study that used a similar GGA+U approach and reported an energy barrier of 0.58 eV [13].

The effect of the ZPE correction is to rigidly shift the classical activation energy (migration barrier E_{barr}) to lower energies by 0.12 eV (see figure 9). Such a treatment, however, is only justified at low temperatures where all atoms can be reasonably assumed to behave as quantum harmonic oscillators confined to their lowest-energy vibrational state. A more rigorous way to include quantum-mechanical corrections is through the Wigner-correction term, δE_{Wigner} [36]. The

modified (with the Wigner correction) activation energy will thus be: $E_a = E_{barr} + \delta E_{Wigner}$. This correction is temperature dependent [36]:

$$\delta E_{Wigner} = -k_B T \ln \left[\frac{\prod_i^{3N} \sinh(x_i^{GS})/x_i^{GS}}{\prod_i^{3N-1} \sinh(x_i^{TS})/x_i^{TS}} \right] \quad (5)$$

where x_i is a quantity which characterizes each vibrational mode i and is given by $h\nu_i/2k_BT$. It can be seen in figure 9 that at higher temperatures the modified (Wigner-corrected) activation energy ($E_{barr} + \delta E_{Wigner}$) approaches the classical migration barrier, whereas at lower temperatures it tends towards the ZPE-corrected activation energy.

The present results for E_a slightly underestimate the experimentally derived activation energies of hydrogen diffusion parallel to the c axis: an activation energy of 0.59 eV was obtained by Johnson *et al* [15] from high-temperature diffusion data (the temperature range was from 350°C–700 °C). A recent work has extended diffusion measurements to lower temperatures (from 157 K to 197 K) by studying stressed-induced dichroism of the local vibrational modes due to hydrogen and deuterium [38]. These authors reported an overall activation energy equal to 0.54 eV by combining high-temperature and low-temperature data. The derived diffusion coefficient parallel to the c axis was equal to: $D_{\parallel}^{exp} = 9.4 \times 10^{-4} \times e^{-0.541/k_BT}$, expressed in units of $cm^2\ s^{-1}$. In the same study activation energies for hydrogen c-axis diffusion were also determined theoretically but the reported results exhibited an even larger underestimation of the experimental values [38]. The origin of this discrepancy very likely originates from the use of the plain GGA functional without on-site U correction. As those authors acknowledged the semilocal GGA functional underestimates the classical barrier E_{barr}. Inclusion of exact Hartree–Fock exchange would improve the DFT-based results. These authors quoted an increase in the migration barrier for hydrogen along the c axis by an amount of 0.09 eV when employing a hybrid functional which includes a portion of exact non-local exchange [38].

The diffusion prefactor can also be obtained from the transition rate, Γ. Assuming a random-walk model of diffusion and movement in one direction, the diffusion coefficient $D_{\parallel}$ parallel to the c axis is proportional to the rate Γ as follows:

$$D_{\parallel} = \frac{d^2}{2}\Gamma, \quad (6)$$

where d represents the jump distance of hydrogen along the prescribed path. For the case of diffusion along the c axis d equals $c/2$. Combining equations (4) with (6) leads to a diffusion prefactor of $2.27 \times 10^{-3}\ cm^2\ s^{-1}$, in fairly good agreement with the experimental diffusion data.

4. Conclusions

The energetics of hydrogen configurations in rutile TiO_2 were examined with the aid of GGA+U calculations. Electronic and atomistic structures of the hydrogen states were analyzed and discussed with respect to previous first-principles results and recent spectroscopic data. From the calculated charge-transition levels and spin-density isosurfaces it is demonstrated that hydrogen in rutile is a deep donor; polaron-like configurations with the excess electron localized at neighboring Ti ions were found to be energetically favored with respect to the structure with a delocalized electron density and the Fermi level at the bottom of the conduction band.

Distinct migration paths of hydrogen were also identified and characterized in detail by means of the NEB method. The calculated energy profiles for these paths show a striking anisotropy in the migration barriers for diffusion along versus perpendicular to the crystallographic c axis. The present results outline the necessity of O–H-bond reorientation in order to achieve hydrogen motion between adjacent c channels. The hopping rate and the diffusion coefficient parallel to the c axis were obtained within transition-state theory and were found to be in good agreement with existing experimental observations.

Acknowledgments

This work was financially supported by (i) FEDER (Programa Operacional Factores de Competitividade COMPETE) and by FCT Portugal—Fundação para a Ciência e Tecnologia under the UID/FIS/04564/2016 and PTDC/FIS/102722/2008 projects. The computer resources of the Department of Physics of the University of Coimbra were used, including the Navigator cluster at the Laboratory for Advanced Computing.

ORCID iDs

A G Marinopoulos https://orcid.org/0000-0002-1951-4832

References

[1] Chester P F and Bradhurst D H 1963 *Nature* **199** 1056–7
[2] DeFord J W and Johnson O W 1983 *J. Appl. Phys.* **54** 889–97
[3] Herklotz F, Lavrov E V and Weber J 2011 *Phys. Rev.* B **83** 235202
[4] Mo L B *et al* 2015 *Sci. Rep.* **5** 17634
[5] Brant A T, Yang S, Giles N C and Halliburton L E 2011 *J. Appl. Phys.* **110** 053714
[6] Bekisli F, Fowler W B and Stavola M 2012 *Phys. Rev.* B **86** 155208
[7] Shimomura K, Kadono R, Koda A, Nishiyama K and Mihara M 2015 *Phys. Rev.* B **92** 075203
[8] Vilão R C, Vieira R B L, Alberto H V, Gil J M, Weidinger A, Lichti R L, Baker B B, Mengyan S P W and Lord J S 2015 *Phys. Rev.* B **92** 081202
[9] Xiong K, Robertson J and Clark S J 2007 *J. Appl. Phys.* **102** 083710
[10] Bjørheim T S, Stølen S and Norby T 2010 *Phys. Chem. Chem. Phys.* **12** 6817–25
[11] Bjørheim T S, Kuwabara A and Norby T 2013 *J. Phys. Chem.* C **117** 5919–30
[12] Li H and Robertson J 2014 *J. Appl. Phys.* **115** 203708
[13] Filippone F, Mattioli G, Alippi P and Bonapasta A A 2009 *Phys. Rev.* B **80** 245203
[14] Deák P, Aradi B and Frauenheim T 2011 *Phys. Rev.* B **83** 155207

[15] Johnson O W, Paekt S H and DeFord J W 1975 *J. Appl. Phys.* **46** 1026–33
[16] Spahr E J, Wen L, Stavola M, Boatner L A, Feldman L C, Tolk N H and Lüpke G 2010 *Phys. Rev. Lett.* **104** 205901
[17] Bates J B, Wang J C and Perkins R A 1979 *Phys. Rev.* B **19** 4130–9
[18] Hohenberg P and Kohn W 1964 *Phys. Rev.* **136** B864–71
[19] Kohn W and Sham L J 1965 *Phys. Rev.* **140** A1133–8
[20] Perdew J P, Burke K and Ernzerhof M 1996 *Phys. Rev. Lett.* **77** 3865–8
[21] Dudarev S L, Botton G A, Savrasov S Y, Humphreys C J and Sutton A P 1998 *Phys. Rev.* B **57** 1505–9
[22] Morgan B J and Watson G W 2010 *J. Phys. Chem.* C **114** 2321–8
[23] Stausholm-Møller J, Kristoffersen H H, Hinnemann B, Madsen G K H and Hammer B 2010 *J. Chem. Phys.* **133** 144708
[24] Jónsson H, Mills G and Jacobsen K W 1998 Nudged elastic band method for finding minimum energy paths of transitions *Classical and Quantum Dynamics in Condensed Phase Simulations* ed B J Berne *et al* (Singapore: World Scientific) pp 385–404
[25] Vineyard G H 1957 *J. Phys. Chem. Solids* **3** 121–7
[26] Blöchl P E 1994 *Phys. Rev.* B **50** 17953–79
[27] Kresse G and Joubert D 1999 *Phys. Rev.* B **59** 1758–75
[28] Kresse G and Hafner J 1993 *Phys. Rev.* B **47** 558–61
[29] Kresse G and Hafner J 1994 *Phys. Rev.* B **49** 14251–69
[30] Kresse G and Furthmüller J 1996 *Phys. Rev.* B **54** 11169–86
[31] Shibuya T, Yasuoka K, Mirbt S and Sanyal B 2012 *J. Phys.: Condens. Matter* **24** 435504
[32] Vos K 1977 *J. Phys. C: Solid State Phys.* **10** 3917–40
[33] Parker R A 1961 *Phys. Rev.* **124** 1719–22
[34] Johnson O W, Ohlsen W D and Kingsbury P I Jr 1968 *Phys. Rev.* **175** 1102–9
[35] Peacock P W and Robertson J 2003 *Appl. Phys. Lett.* **83** 2025–7
[36] Henkelman G, Arnaldsson A and Jónsson H 2006 *J. Chem. Phys.* **124** 044706
[37] Koudriachova M V, de Leeuw S W and Harrison N M 2004 *Phys. Rev.* B **70** 165421
[38] Hupfer A J, Monakhov E V, Svensson B G, Chaplygin I and Lavrov E V 2017 *Sci. Rep.* **7** 17065
[39] Cox S F J 2009 *Rep. Prog. Phys.* **72** 116501